

BIDIRECTIONAL DUAL-ACTIVE BRIDGE DC-DC CONVERTER USING A
MATRIX TRANSFORMER

by

Faisal Alamri

A thesis submitted to the faculty of
The University of North Carolina at Charlotte
in partial fulfillment of the requirements
for the degree of Master of Science in
Electrical Engineering

Charlotte

2023

Approved by:

Dr. Babak Parkhideh

Dr. Dipankar Maity

Dr. Maciej Noras

ABSTRACT

FAISAL ALAMRI. Bidirectional Dual-Active Bridge DC-DC converter using a Matrix Transformer. (Under the direction of DR. BABAK PARKHIDEH)

Dual Active Bridge (DAB) converter is an advanced power electronics device with various applications in renewable energy systems, electric vehicles, and high-power energy conversion systems. Due to its versatility and critical role in modern power electronics, the DAB converter has become essential in different technology areas.

The topology of DAB converters has been continuously improving in terms of higher efficiency, increased power density, and expanding diversity of applications. Today, DAB converter topology is used in renewable energy systems, energy Storage Systems, and smart grid applications.

This thesis provides a detailed analysis of the DAB converter topology, including its state-space representation, SPS control logic, design, averaging, and linearization. The purpose is to comprehensively explore the DAB converter, understand its dynamic behavior and operation states, analyze its control strategies, and acknowledge its wide range of applications.

DEDICATION

This thesis is dedicated to my grandfather, Theyab Saeed Alamri, for his extraordinary encouragement for education that sparked my passion for higher-learning and academic pursuits.

ACKNOWLEDGEMENTS

I am incredibly grateful to my advisor, Dr. Babak Parkhideh, for his unwavering support and guidance during my thesis. His brilliant insights and illuminating discussions on the field of power electronics have been invaluable to my work.

I also want to express my heartfelt thanks to the committee members, Dr. Dipankar Maity and Dr. Maciej Noras, who generously provided me with constructive feedback on my work and patiently answered my countless questions despite their busy schedules.

I also would like to express my special gratitude for Nasser Althaiban, and all my friends for their help and patience while working on this thesis and for the fun and insightful conversations we had.

Special thanks to the Energy Production and Infrastructure Center (EPIC) research team for their invaluable supervision and early-stage insights. Additionally, I gratefully acknowledge the financial support provided by GASP.

Lastly, I would like to extend my deepest and wholeheartedly gratitude to my parents, Abdulmajeed Alamri and Norah Alamri for their endless financial and emotional support throughout my academic and personal life. I cannot express how grateful I am for all they have sacrificed to make this journey possible.

TABLE OF CONTENTS

LIST OF TABLES	viii
LIST OF FIGURES	ix
LIST OF ABBREVIATIONS	xi
LIST OF SYMBOLS	xv
CHAPTER 1: INTRODUCTION	1
CHAPTER 2: LITERATURE REVIEW	3
CHAPTER 3: METHODOLOGY	6
3.1. AC Power Transfer	6
3.2. Inductor Voltage Analysis	8
3.3. Inductor Current Analysis	11
3.4. Conversion Ratio	11
3.5. Design Parameters	13
3.6. Power Losses	15
3.6.1. Application of ZVS	16
3.6.2. Application of ZCS	20
CHAPTER 4: CONTROL LOGIC	21
4.1. State-space Design	22
4.2. State-space averaging and linearization	26
4.3. Transfer function	29
CHAPTER 5: RESULTS	31
5.1. Simulation Results	35

	vii
5.2. Varying Load and Input Voltage Conditions	38
CHAPTER 6: CONCLUSIONS	42
REFERENCES	44
APPENDIX A: CAPACITOR SIZING CALCULATION	46
APPENDIX B: STATE-SPACE PERTURBING AND LINEARIZATION	49

LIST OF TABLES

TABLE 3.1: Time segment table for ON gates.	10
TABLE 4.1: Operating states time periods for DAB converter.	27
TABLE 5.1: Converter Specifications for Simulink	34
TABLE 5.2: Summary for different testing conditions	41

LIST OF FIGURES

FIGURE 3.1: AC representation of DAB converter	6
FIGURE 3.2: DAB Converter Circuit	8
FIGURE 3.3: Voltage Sources Waveform	9
FIGURE 3.4: Inductor Voltage Waveform	10
FIGURE 3.5: Inductor Current Waveform	11
FIGURE 3.6: Output Current Waveform	12
FIGURE 3.7: Duty Ratio Operating Range	14
FIGURE 3.8: Power Switching Losses	16
FIGURE 3.9: Operating Devices During Stage A	16
FIGURE 3.10: Stage A Time Interval of the Inductor Current	17
FIGURE 3.11: Operating Devices During Stage B	17
FIGURE 3.12: Stage B Time Interval of the Inductor Current	18
FIGURE 3.13: Time Instance of the ZVS Application	18
FIGURE 3.14: DAB converter Equivalent Circuit operating at ZVS	19
FIGURE 3.15: ZCS Application on the Inductor Current	20
FIGURE 4.1: Open-loop System Representation	21
FIGURE 4.2: Closed-loop System Representation	22
FIGURE 4.3: Inductor Voltage Waveform	24
FIGURE 4.4: DAB converter equivalent circuits for each operating states.	24
FIGURE 4.5: DAB converter equivalent circuits for each operating states.	25
FIGURE 5.1: DAB Converter Simulation Circuit	31

FIGURE 5.2: Simulation Control Unit	32
FIGURE 5.3: Simulation Control Block Diagram	32
FIGURE 5.4: Phase Shifting Logic Subsystem of the Control Block Diagram	33
FIGURE 5.5: Simulation Switching Devices Signals	33
FIGURE 5.6: Simulation Scoping Probes	34
FIGURE 5.7: Simulation for Output Measurement at Nominal Load	35
FIGURE 5.8: Simulation Transformer Measurements at Nominal Load	36
FIGURE 5.9: Simulation Transformer Waveform Characteristics	37
FIGURE 5.10: Output Measurements for Nominal Load Testing Condition.	38
FIGURE 5.11: Output Measurements for Mid-point Load Testing Condition.	39
FIGURE 5.12: Output Measurements for No Load Testing Condition.	39
FIGURE 5.13: Output Measurements for 10% Input Voltage increment Testing Condition.	40
FIGURE 5.14: Output Measurements for 20% Input Voltage increment Testing Condition.	41
FIGURE A.1: ΔQ Calculation	47

LIST OF ABBREVIATIONS

CMC	Current Mode Control
DAB	Dual-Active Bridge
DPS	Dual Phase Shift
EPS	Extended Phase Shift
EV	Electric Vehicle
HFL	High Frequency Link
KVL	Kirchhoff's Voltage Law
PCS	Power Conversion System
PWM	Pulse Width Modulation
SPS	Single Phase Shift
TPS	Triple Phase Shift
VMC	Voltage Mode Control

LIST OF SYMBOLS

A	State Matrix
B	Input Vector
C_o	Output Capacitor
$[C_1 - C_8]$	Snubber Capacitors
C_{oss}	Snubber Capacitor
D	Duty Ratio
\hat{d}	Duty Ratio small-signal perturbation
E	Control Coefficient
f_{sw}	Switching Frequency
G	Output Matrix
G_{vd}	Control-to-output Transfer Function
G_{vg}	Line-to-output Transfer Function
H	Direct Transmission Matrix (Feedthrough Matrix)
I	Identity Matrix
I_1	DC Primary Current
I_2	DC Secondary Current
i_1	AC Primary Current

i_2	AC Secondary Current
I_D	Drain Current
I_o	DC Output Current
\hat{i}_L	Inductor Current small-signal perturbation
L	Leakage Inductor
M	Conversion Ratio
n	Transformer Ratio
P_2	Output Power
P_{avg}	Power Average
P_{Loss}	Power Loss
Q	Capacitor Charge
R_L	Load Resistance
s	Laplace Transformation
$[S1 - S8]$	Switching Devices
T_{on}	Turn-on Delay time of the switch
T_s	Switching Period
t_1	time period
t_2	time period

t_d	Dead Time
U_0	DC Input Vector term
u	Input Vector
V_1	DC Primary Voltage
V_2	DC Secondary Voltage
v_1	AC Primary Voltage
v_2	AC Secondary Voltage
V_C	DC Capacitor Voltage
v_C	AC Capacitor Voltage
V_{DS}	Drain-to-Source Voltage
V_g	DC Input Voltage
V_{in}	DC Primary Voltage
V_o	DC Output Voltage
\hat{v}_C	Capacitor voltage small-signal perturbation
$\langle V_L \rangle$	Average Inductor Voltage
\hat{v}_g	Input voltage small-signal perturbation
x	State Vector
X_0	DC State Vector term

\dot{x}	State Vector small-signal perturbation
y	Output Vector
Δ	Greek Letter
ω	Greek Letter
ϕ	Greek Letter
Σ	Greek Letter
θ	Greek Letter

CHAPTER 1: INTRODUCTION

The Dual Active Bridge (DAB) converter is a highly advanced power electronics device that finds use in several applications, such as renewable energy systems, electric vehicles, and high-power energy conversion systems. Its primary function is to control the conversion of electrical energy between two different DC voltage sources with high efficiency and precision. Due to its versatility and critical role in modern power electronics, the DAB converter has become essential in different technology areas. The summary of the thesis chapters is listed in this section, where the DAB converter is analyzed.

CHAPTER 2 provides a literature review briefing and discusses the system construction and topology components, control logic implementation for DAB converter topology, state-space modeling, design and linearization, software modeling, challenges and future directions, and conclusion.

CHAPTER 3 explains the methodology for implementing the DAB converter topology. It starts by analyzing the AC power flow transformation of the basic yet equivalent circuitry of the DAB converter. Then, it examines the inductor voltage and current, showing the converter behavior over a cycle period. After that, the conversion ratio is calculated, which expresses and explains the converter behavior from different perspectives. Moreover, the power losses of the switching devices are addressed, and the application of zero-voltage-switching (ZVS) and zero-current-switching (ZCS) is discussed as a solution to the problem.

CHAPTER 4 proposes the control logic of the DAB converter, and the state-space model design is constructed. Furthermore, the state-space averaging process and the line-to-output and control-to-output transfer functions are also calculated.

CHAPTER 5 presents the simulation results using Simulink and the experimental results for the specifications provided.

Finally, CHAPTER 6 concludes the thesis by comparing the results and discussing future work and plans for this DAB converter.

CHAPTER 2: LITERATURE REVIEW

DC-DC converters have been playing a crucial role in a wide range of applications in power electronics. It has upgraded the efficiency level and provided more features for users, such as stepping up or down voltage and current, reducing parasitic component sizes, transforming higher power density, advancing switching frequency control, and performing bidirectional power flow transmission. DAB converters have been a well-known topic for their powerful features and highly efficient performance, initially proposed in [1]. It also provides various applications in electric vehicles (EVs) [2], aerospace applications [3], data centers [4].

As mentioned, DAB converter was initially proposed in 1988 [1]. The topology of DAB converters has been continuously improving in terms of higher efficiency, increased power density, and expanding diversity of applications. Today, DAB converter topology is used in renewable energy systems, energy Storage Systems, and smart grid applications. Presented accordingly in [5, 6, 7].

The DAB converter consists of two full bridges. The first bridge is an inverter connected to the input, which converts DC to AC. The second bridge is a rectifier connected to the output, which converts AC back to DC. It also consists of an inductor, which controls the direction of power flow, and often a transformer, primarily for isolation and for stepping up or down voltage and current. Similarly, many researchers have discussed improvements in the DAB converter topology, such as separating the windings of the leakage inductance presented in [8], using the dual transformer discussed in [9], and operating the DAB converter without the transformer introduced

in [10].

Numerous research studies have been conducted on the control of DAB converter topology. For instance, one research paper in [1] discusses a soft-switched DAB converter and other bidirectional DC-DC converters suitable for high-power density applications. The study compares DC-DC topologies, such as single-phase-shifted, single-phase, and three-phase dual bridge converter topologies. In [11], voltage-mode-control (VMC) and current-mode-control (CMC) methods were discussed, where CMC was implemented using voltage reference error. Additionally, [12] discusses the short-time-scale transient processes in an isolated bidirectional DAB converter with a phase-shifted control. The study analyzed the dead-band effect on the steady-state and transient commutating process. In addition, High-frequency-link (HFL) power conversion systems (PCSs) control was discussed in [13], which compares the implementation of single-phase-shift (SPS), extended-phase-shift (EPS), dual-phase-shift (DPS), and triple-phase-shift (TPS) as well. Each of these implementations of phase-shifting methods was discussed thoroughly in [14, 15, 16, 17].

State-space modeling is a sophisticated technique for averaging and linearizing systems, which is also easy to apply to a DC-DC system like a DAB converter topology. A comprehensive guide for state-space design and modeling can be found in [18]. Additionally, [19] and [20] discuss state-space averaging and linearizing, providing all the state-space components, the averaging process, and a transfer function for the DAB converter system.

In the MATLAB workspace, a comprehensive model design work for DAB has been completed using the Simulink tool. The model includes measurements and tests of different operating scenarios and conditions for the DAB converter system. The find-

ings from this model will be further explored in this thesis.

The DAB converter topology is more complex than other converters because it functions on more than two operating states, such as Buck, Boost, Buck-boost, and others. This complex behavior of the DAB converter topology makes the control logic much more complicated. However, the control logic can be analyzed and calculated by redefining the operating states of the DAB converter, as shown in [3] and [19].

Due to design limitations, the research was limited to a down-scaled version. Nonetheless, in the future, these limitations will be overcome to implement the full scale and achieve the full output power as stated in the objectives of this project.

As discussed earlier, the topology of DAB converters is a rapidly evolving field that has resolved numerous issues and provided significant advantages in the realm of power electronics. DAB converters have become indispensable to several global projects, including electric vehicles and DC circuit breakers [21].

CHAPTER 3: METHODOLOGY

3.1 AC Power Transfer

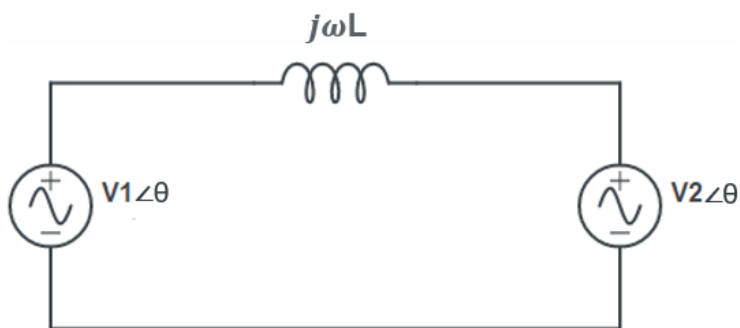


Figure 3.1: AC representation of DAB converter

Using this simple circuit to represent the AC power transfer in DAB converter topology, the power transfer could be analyzed as the first AC source V_1 going through the inductor $j\omega L$, and the other AC source V_2 . V_1 and V_2 AC voltage sources could either produce or absorb voltage depending on their phase angle degree. Having fixed 0° phase degree for V_1 , and changing the phase angle degree for V_2 , would control the power transfer through the converter. If V_2 phase angle is > 0 , the current path would be from V_1 toward V_2 where V_1 would be a producing source and V_2 would be an absorbing source. The current would be in the other direction if V_2 phase angle is negative < 0 where V_1 would be an absorbing source and V_2 would be a producing source. V_1 and V_2 voltage sources could be expressed as two cosine waveforms as follows:

$$V_1 = v_1(t)\cos(\omega t - 0) \quad (3.1)$$

$$V_2 = v_2(t)\cos(\omega t - \theta) \quad (3.2)$$

Current could be calculated using:

$$I(t) = \frac{v_1(t) - v_2(t)}{j\omega L} \quad (3.3)$$

$$I(t) = \frac{v_1(t)}{\omega L} \sin(\omega t) - \frac{v_2(t)}{\omega L} \sin(\omega t - \theta) \quad (3.4)$$

Therefore, the output power calculation would be:

$$p_2 = v_2(t) i_2(t) \quad (3.5)$$

$$p_2 = v_2(t) \cos(\omega t - \theta) \left(\frac{v_1(t)}{\omega L} \sin(\omega t) - \frac{v_2(t)}{\omega L} \sin(\omega t - \theta) \right) \quad (3.6)$$

Calculating the average output power:

$$P_{avg} = \int_0^T p_2(t) dt \quad (3.7)$$

$$P_{avg} = \frac{V_1 V_2}{2\omega L} \frac{1}{T} \int_0^T \cos(\omega t - \theta) \sin(\omega t) dt \quad (3.8)$$

$$P_{avg} = \frac{V_1 V_2}{2\omega L} \sin(\theta) \quad (3.9)$$

From this, we could realize that θ plays a crucial role to control the average power between the AC voltage sources.

Since the DAB converter is a DC-DC converter, two active bridges that contain eight active switches such as MOSFETs, SiCs, IGBTs or many other switching devices,

are required to convert AC source to a DC source. In addition, a transformer will be used for isolation, step-up, and step-down, and two capacitors at both ends will be constructed for filtering DC ripple. Because we have an inductor in the DAB converter simple circuit topology, and using a transformer, would result in having a "real transformer" where the leakage inductance of the transformer is used.

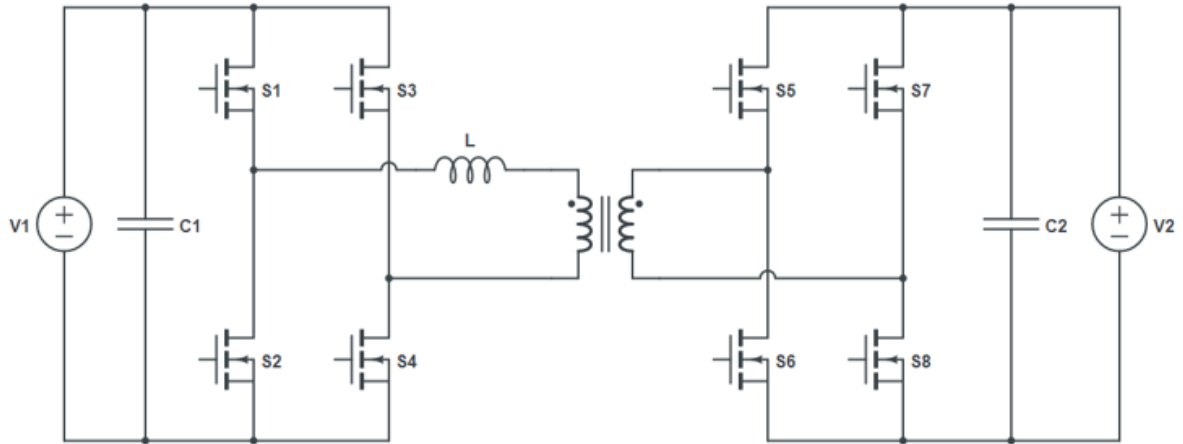


Figure 3.2: DAB Converter Circuit

3.2 Inductor Voltage Analysis

Drawing V_1 and V_2 voltage waveforms with the assumptions that V_1 is higher than V_2 , the Duty Cycle is 50%, and there is ϕ phase shift for V_2 would be:

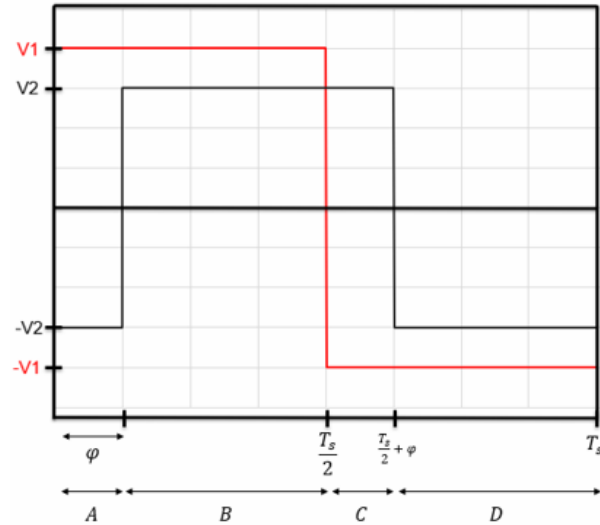


Figure 3.3: Voltage Sources Waveform

As shown above, V_1 is the red square waveform where it operates high at the interval $\{0 \text{ to } \frac{T_s}{2}\}$ and low at the interval $\{\frac{T_s}{2} \text{ to } T_s\}$. V_2 is the black square waveform and, it is phase shifted by ϕ , and it operates high at the interval $\{\phi \text{ to } (\frac{T_s}{2} + \phi)\}$ and low for the interval $\{(\frac{T_s}{2} + \phi) \text{ to } (T_s + \phi)\}$.

In addition, the period of time segments are noted as A, B, C, D, whereas they indicate what switches were on at that period of time. Here is a truth-table of these notation.

Table 3.1: Time segment table for ON gates.

Time Segment	Primary Bridge	Secondary Bridge
	Switches ON	
A	S1, S4	S6, S7
B	S1, S4	S5, S8
C	S2, S3	S5, S8
D	S2, S3	S6, S7

After combining the the voltage sources waveform and following Kirchhoff's voltage law (KVL) $\langle V_L \rangle = V_g - V_o$, the inductor voltage waveform result will be:

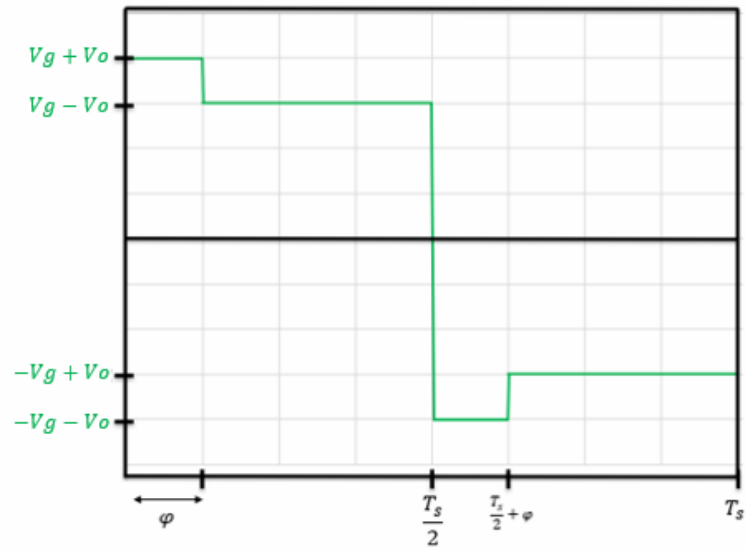


Figure 3.4: Inductor Voltage Waveform

3.3 Inductor Current Analysis

Since the average inductor current is 0, we could use the inductor voltage waveform to draw the inductor current waveform using Kirchhoff's current law (KCL)

$\langle i_L \rangle = \frac{V_g - V_o}{L}$. Using this method, the inductor current waveform result will be:

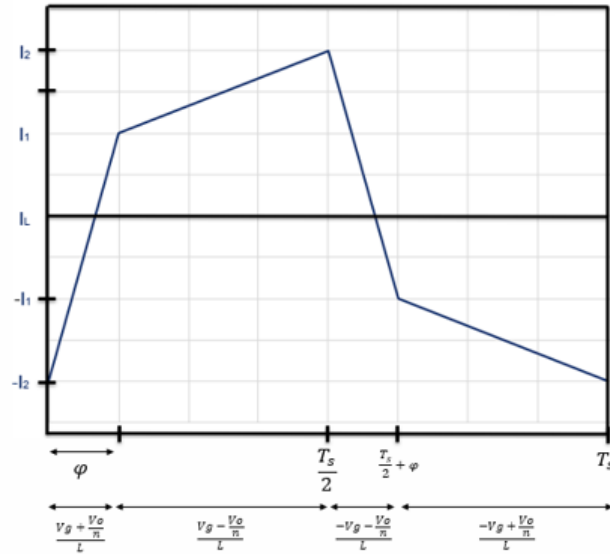


Figure 3.5: Inductor Current Waveform

3.4 Conversion Ratio

In order to find the conversion ratio $M = \frac{V_o}{V_{in}}$, the output current must be found. The output current waveform is going to be similar to the inductor current except that it would be rectified as shown below.

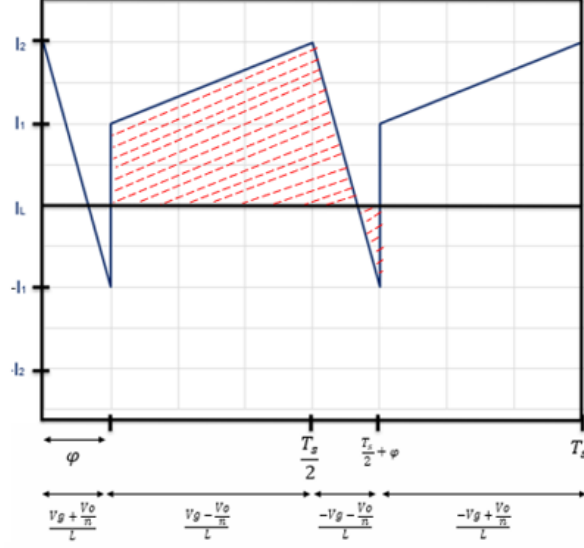


Figure 3.6: Output Current Waveform

Using this waveform, we could calculate the output current I_o by calculating the area under the curve. The average of the output current is achievable by calculating the amount of the output charge where the output current is:

$$I_o = \frac{\Delta Q}{n \frac{T_s}{2}} \quad (3.10)$$

$$\Delta Q = \frac{1}{2}(I_1 + I_2) \left(\frac{T_s}{2} - \phi \right) + \frac{1}{2}t_1(I_2) - \frac{1}{2}t_2(I_1) \quad (3.11)$$

Where t_1 , t_2 are used here to represent the first and second half of the first time segment $\frac{V_g + V_o/n}{L}$. Therefore,

$$t_1 = \frac{I_2 L}{V_g + \frac{V_o}{n}} \quad (3.12)$$

$$t_2 = \frac{I_1 L}{V_g + \frac{V_o}{n}} \quad (3.13)$$

Solving for ΔQ using t_1 and t_2 :

$$\Delta Q = \phi \left(\frac{T_s}{2} - \phi \right) \frac{V_g}{L} \quad (3.14)$$

Using the previous formula $I_o = \frac{\Delta Q}{n \frac{T_s}{2}}$:

$$I_o = \frac{\phi \left(\frac{T_s}{2} - \phi \right) V_g}{n \frac{T_s}{2} L} = \frac{\phi \left(1 - \frac{2\phi}{T_s} \right) V_g}{n L} \quad (3.15)$$

Using:

$$D = \frac{2\phi}{T_s}, \quad f_{SW} = \frac{1}{T_s} \quad (3.16)$$

I_o would become as:

$$I_o = \frac{D(1-D)V_g}{n f_{SW} L} \quad (3.17)$$

Using Ohm's law:

$$I_o = \frac{V_o}{R_L} = \frac{D(1-D)V_g}{n f_{SW} L} \quad (3.18)$$

By equating these two equation, the conversion ratio could be expressed as:

$$m = \frac{V_o}{V_g} = \frac{D(1-D)R_L}{n f_{SW} L} \quad (3.19)$$

3.5 Design Parameters

Duty ratio is a crucial variable in the design section. By looking at the graph of the duty ratio:

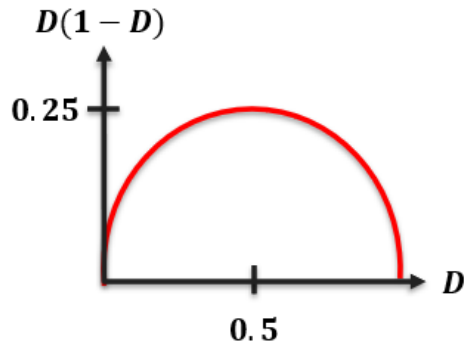


Figure 3.7: Duty Ratio Operating Range

The converter transfers the maximum power at $D = 0.5$. However, in this design, D is chosen to be equal to 0.4 instead, to avoid control issues and to provide room for transients.

Having the conversion ratio equation, we could calculate the size of the leakage inductance should be used in the converter to acquire maximum efficiency.

The leakage inductance could be calculated as:

$$L = \frac{D(1-D)R_L V_g}{n f_{sw} V_o} \quad (3.20)$$

Furthermore, the output capacitance could be calculated using the output current waveform I_o (Figure 3.6) and could be calculated as:

$$C_o = \frac{\Delta Q}{2 \Delta V_o} \quad (3.21)$$

where,

$$\Delta Q = \frac{V_g D^2 T_s^2}{2 f_{sw} L n} \quad (3.22)$$

The derivation and calculation of ΔQ is provided in APPENDIX A.

3.6 Power Losses

High operating frequencies will reduce the size of passive elements such as capacitors, inductors, and power transformers. Although, operating at high frequencies is beneficial for reducing the passive components size, running DC-DC converter topologies using active switches will operate in hard-switching mode. Hard-switched Pulse-Width-Modulated (PWM) converter topologies are easier to analyze however they have a significant power losses that would have a great impact on the converter efficiency.

Soft switching - such as Zero-voltage-switching and Zero-current-switching - are effectively sufficient solution for switching power losses where they are considered in this section to be addressed and applied to DAB converter topology later in this section.

In the next figure, the concept of hard-switching is presented where it shows the principle of hard-switching and how it occurs. Once the switch starts to conduct (turned-on), the conduction of current I_D rises and the drain to source voltage V_{DS} falls both at the same time.

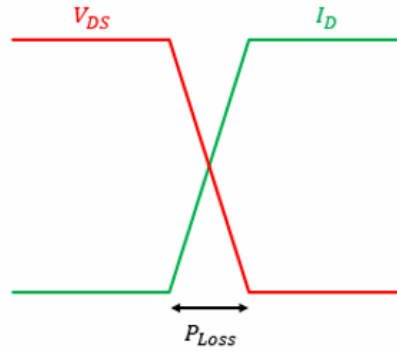


Figure 3.8: Power Switching Losses

This change of event creates a triangle of power loss where it could be calculated using the following formula:

$$P_{Loss} = \frac{1}{2} V_{DS} I_D T_{on} f_{SW} \quad (3.23)$$

3.6.1 Application of ZVS

To implement ZVS soft-switching technique, the inductor current must be analyzed for each operating state as follows:

In the first time segment of the operating state (A), the current path across the circuit would be as:

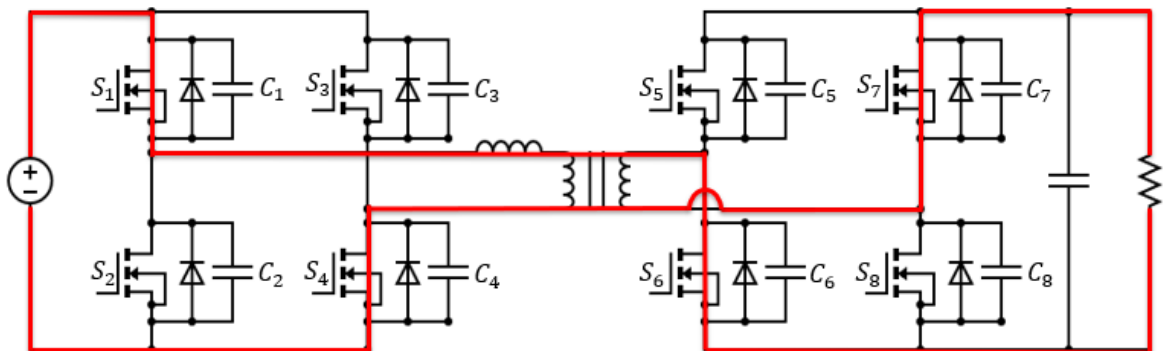


Figure 3.9: Operating Devices During Stage A

Which corresponds to the highlighted time segment of the inductor current waveform below:

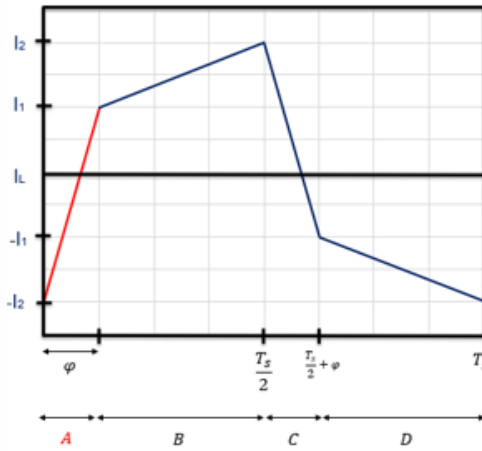


Figure 3.10: Stage A Time Interval of the Inductor Current

At this state, S_1 , S_4 , S_6 , and S_7 devices gates are ON. Simultaneously, the MOSFET output capacitors C_2 and C_3 will be charged by V_{in} value and, C_5 and C_8 will be charged by V_o value.

In the second time segment of the operating state (B), the current path across the circuit would be as:

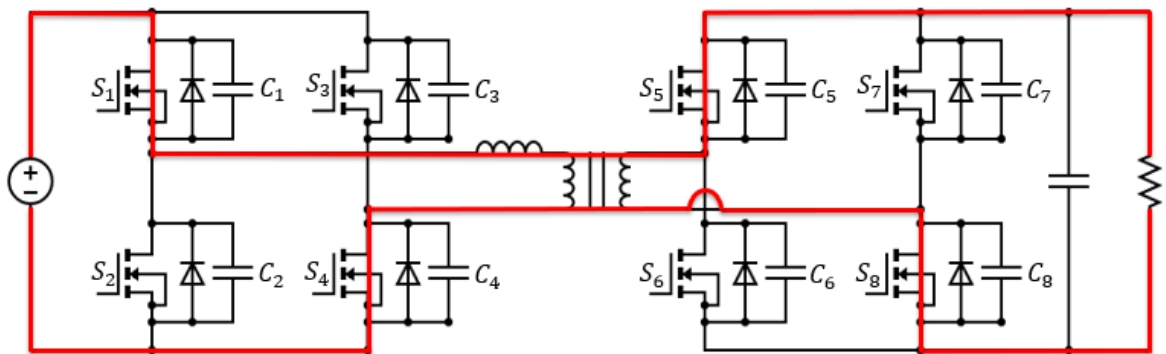


Figure 3.11: Operating Devices During Stage B

Which corresponds to the highlighted time segment of the inductor current waveform below:

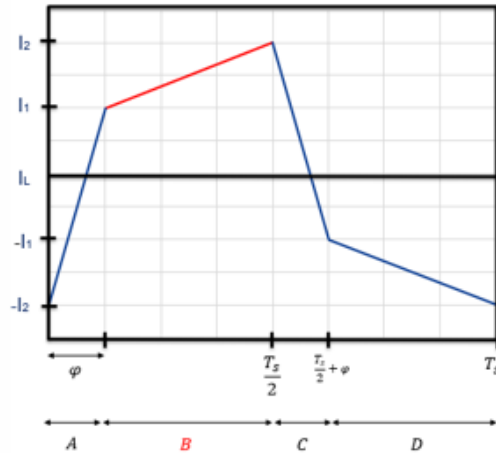


Figure 3.12: Stage B Time Interval of the Inductor Current

At this state, S_1 , S_4 , S_5 , and S_8 devices gates are ON. Simultaneously, the MOS-FET output capacitors C_2 and C_3 will be charged by V_{in} value and, C_6 and C_7 will be charged by V_o value.

The application of ZVS happens at the point of time between A and B operating states.

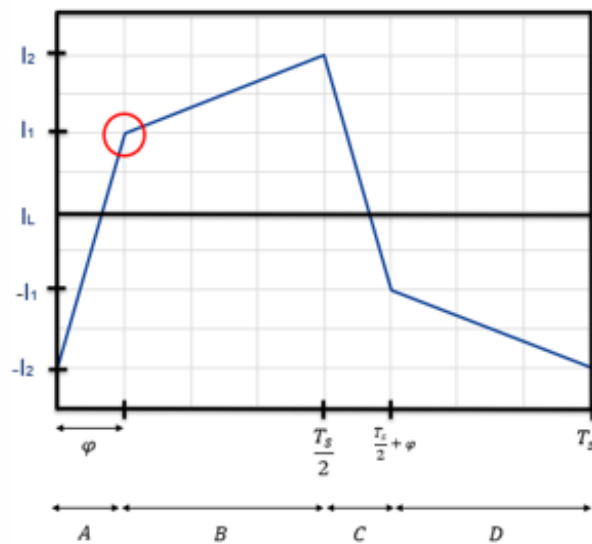


Figure 3.13: Time Instance of the ZVS Application

At this point of time, a short dead-time period will occur where all switching devices

will be turned-off to avoid any short circuit. In addition, applying dead-time at this period of time will result in having a natural commutation by the inductor current that will force the diodes to commutate as they will act as voltage sources via the series capacitors.

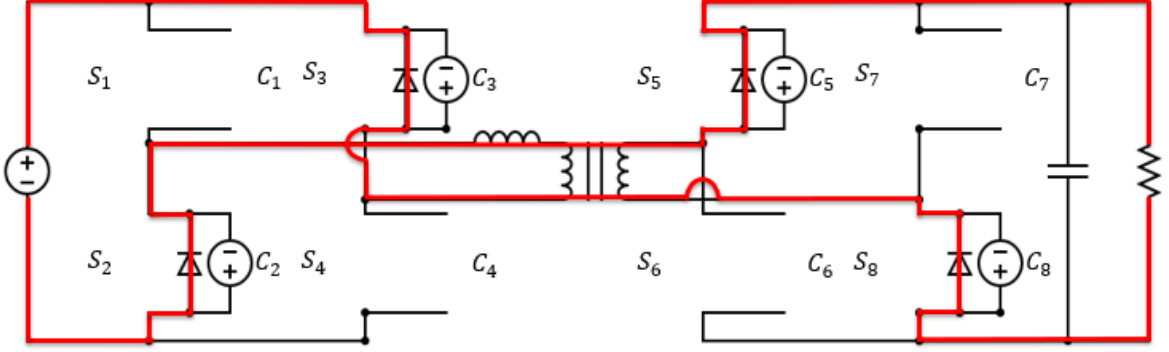


Figure 3.14: DAB converter Equivalent Circuit operating at ZVS

Using the previous power loss formula, and implying this process of ZVS, the power loss formula becomes as:

$$P_{Loss} = \frac{1}{2} V_F I_L t_d f_{SW} \quad (3.24)$$

The drain-to-source voltage V_{DS} and the drain current I_D become as forward voltage drop of the diode V_F and the inductor current I_L . Moreover, t_d here corresponds to the delay time "dead-time" which could be controlled.

Dead-time t_d must be calculated correctly to achieve ZVS efficiently such as:

$$\Delta V = V_o = \frac{\Delta Q}{\sum C_{oss}} = \frac{I_L t_d}{C_5 + C_8} \quad (3.25)$$

$$t_d = \frac{V_o}{I_L} (C_5 + C_8) \quad (3.26)$$

3.6.2 Application of ZCS

In addition, ZCS is another method for soft-switching where it could be used in DAB converters via utilizing the zero-crossing points of the inductor current showing below.

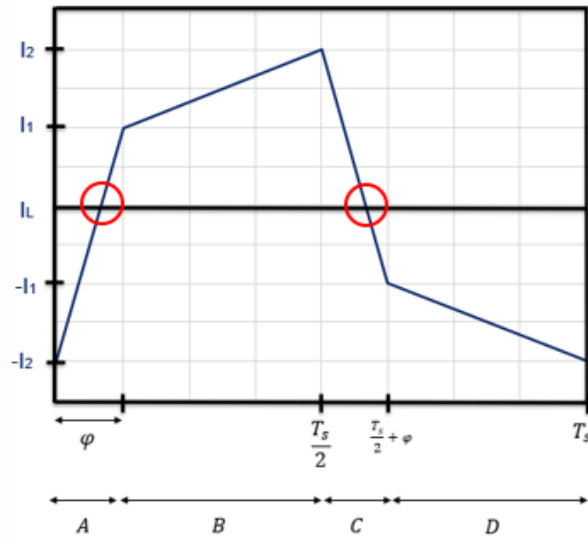


Figure 3.15: ZCS Application on the Inductor Current

Using the control variable to precisely utilize these points to switch the active devices will enforce the switches to operate under ZCS where $I_D = 0$ in the power loss formula mentioned previously. However, operating the active devices under ZCS will cause the phase-shifting control to be used for switching the active devices at the zero-crossing points. Alternatively, duty ratio could be used as a control variable to control the output voltage or current.

CHAPTER 4: CONTROL LOGIC

Control in power electronics involves the implementation of various techniques and strategies to regulate and manage the electrical power output of electronic devices. It also ensures the power of electronic devices' efficiency and reliability in many applications. Regulation and correction of electrical energy is a critical key of control methods in the power electronics principle.

Moreover, the objective of the control in power electronics is to achieve the desired output, such as voltage, current, or frequency. In addition, it is important that the system operates in a manner that meets the requirements expected from the system.

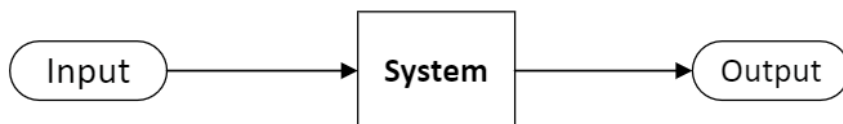


Figure 4.1: Open-loop System Representation

Open-loop systems contain three main blocks: the input, the system, and the output. In open-loop systems, no feedback is taken from the output state; therefore, there is no control.

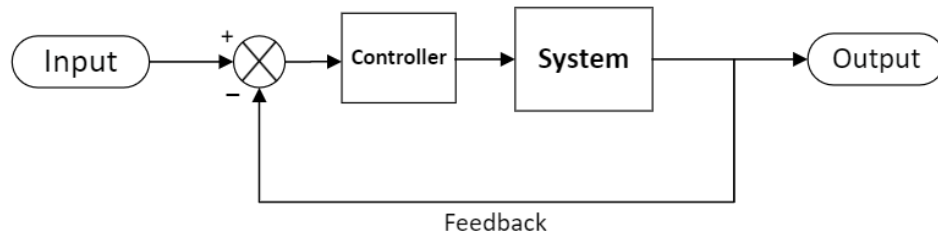


Figure 4.2: Closed-loop System Representation

However, in a closed-loop system, feedback is essential to monitor and regulate the output by calculating the error between the input (Reference) and the output feedback, feeding that into a controller designed by the developer, which would be fed to the system. This process ensures a precise and fine control of the output to be regulated.

4.1 State-space Design

State-space modeling is a mathematical analysis and derivations utilized to describe the behavior of the system dynamics. It provides a sufficient representation that describes the functionality of the system over time.

A state-space model describes a dynamic system by a set of first-order differential equations that define its evolution over time. The critical elements of a state-space model are the state variables, input variables, output variables, and the system matrices.

The state-space modeling comprises of two sets of equations:

- State Equations:

$$\dot{x}(t) = Ax(t) + Bu(t) \tag{4.1}$$

Here, $\dot{x}(t)$ represents the derivative of the state vector with respect to time, A is the state matrix, B is the input matrix, $u(t)$ is the input vector, and $x(t)$ is the state vector.

- Output Equations:

$$y(t) = Gx(t) + Hu(t) \quad (4.2)$$

Here, G is the output matrix, H is the direct transmission matrix or known as (feedthrough matrix), and $y(t)$ is the output vector.

State-space models have several advantages, including the ability to represent systems with multiple inputs and outputs, handle time-varying systems, and facilitate the analysis of system behavior in terms of state trajectories. They are widely used in control system design, system identification, and simulation.

A and B matrices must be constructed to create the state-space design, and x and u vectors must also be identified for the control input. The DAB converter waveform conducts four operating state segments, identified here as A, B, G, and H, which will play a crucial role in the control periods. Therefore, each operating state -as seen below in the inductor voltage i_L - must be analyzed.

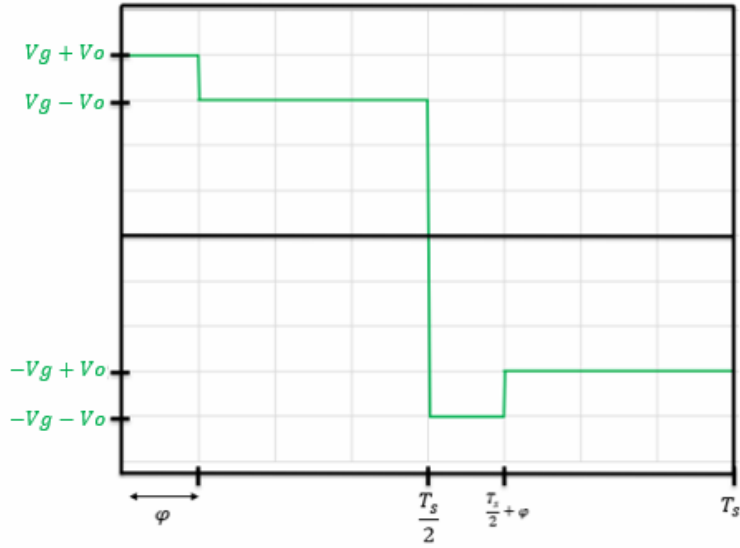


Figure 4.3: Inductor Voltage Waveform

In order to find A and B matrices, the power flow for each state must be analyzed considering only the conductive (ON gates) devices using the ON gates devices table as:

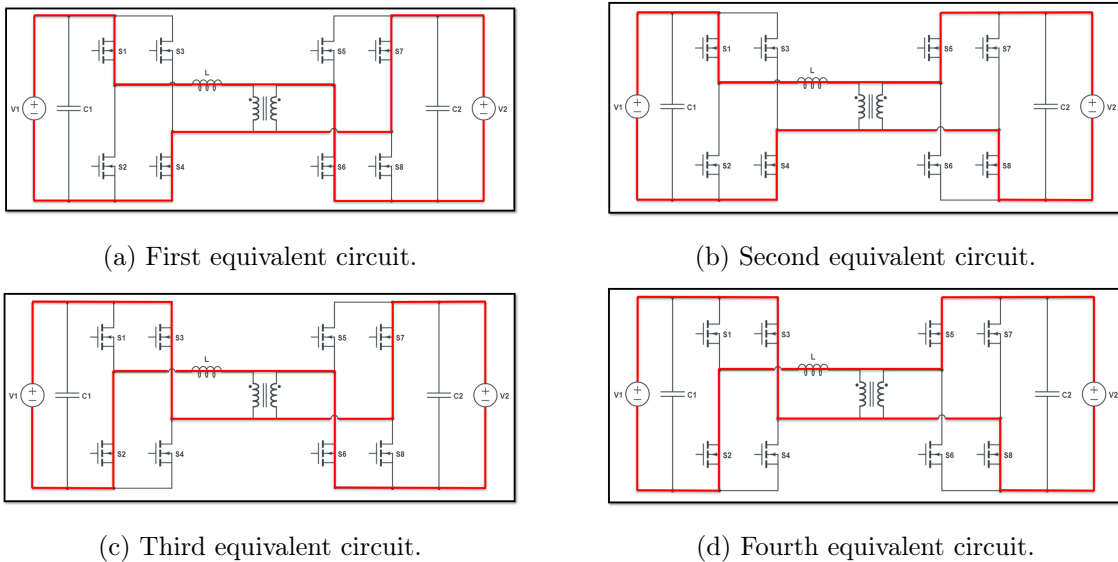


Figure 4.4: DAB converter equivalent circuits for each operating states.

The equivalent circuit for these the figures would be:

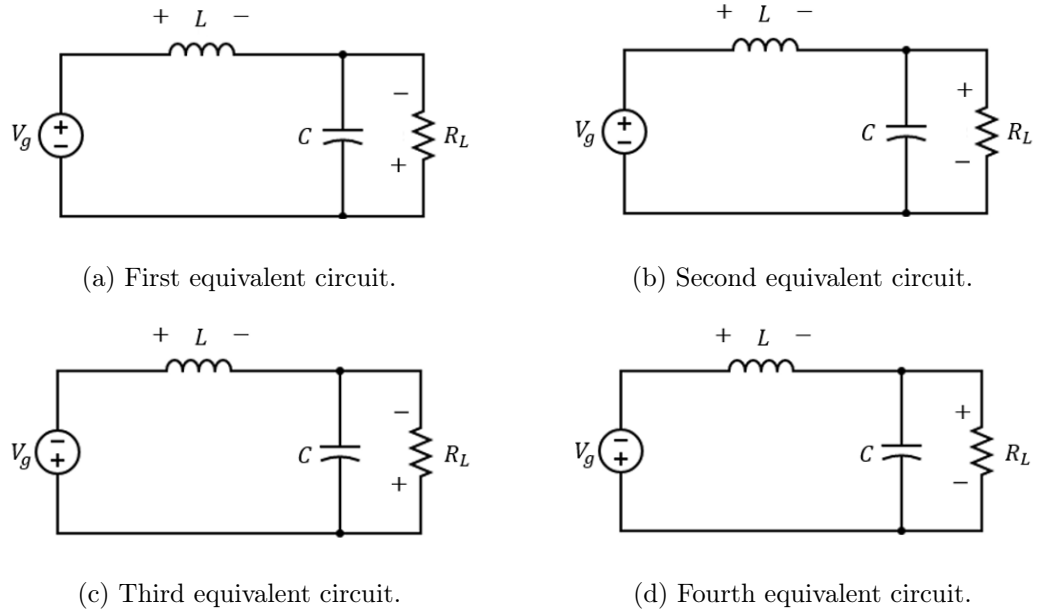


Figure 4.5: DAB converter equivalent circuits for each operating states.

Using these drawings to calculate for the inductor voltage and capacitor current differential equations:

For S_1 :

$$L \frac{di_L(t)}{dt} = V_g + V_o \quad (4.3)$$

$$C \frac{dv_C(t)}{dt} = i_L - \frac{v_C}{R_L} \quad (4.4)$$

For S_2 :

$$L \frac{di_L(t)}{dt} = V_g - V_o \quad (4.5)$$

$$C \frac{dv_C(t)}{dt} = i_L - \frac{v_C}{R_L} \quad (4.6)$$

For S_3 :

$$L \frac{di_L(t)}{dt} = -V_g + V_o \quad (4.7)$$

$$C \frac{dv_C(t)}{dt} = i_L - \frac{v_C}{R_L} \quad (4.8)$$

For S_4 :

$$L \frac{di_L(t)}{dt} = -V_g - V_o \quad (4.9)$$

$$C \frac{dv_C(t)}{dt} = i_L - \frac{v_C}{R_L} \quad (4.10)$$

Using state-space design to envelope these differential equation into matrices and multiplying them by their vectors where:

$$x = \begin{bmatrix} i_L \\ v_C \end{bmatrix}, \quad u = v_g \quad (4.11)$$

This would eventually result into these matrices:

$$A_1 = \begin{bmatrix} 0 & \frac{1}{L} \\ \frac{1}{C} & -\frac{1}{CR_L} \end{bmatrix} \begin{bmatrix} i_L \\ v_C \end{bmatrix}, \quad B_1 = \begin{bmatrix} \frac{1}{L} \\ 0 \end{bmatrix} v_g \quad (4.12)$$

$$A_2 = \begin{bmatrix} 0 & -\frac{1}{L} \\ \frac{1}{C} & -\frac{1}{CR_L} \end{bmatrix} \begin{bmatrix} i_L \\ v_C \end{bmatrix}, \quad B_2 = \begin{bmatrix} \frac{1}{L} \\ 0 \end{bmatrix} v_g \quad (4.13)$$

$$A_3 = \begin{bmatrix} 0 & \frac{1}{L} \\ \frac{1}{C} & -\frac{1}{CR_L} \end{bmatrix} \begin{bmatrix} i_L \\ v_C \end{bmatrix}, \quad B_3 = \begin{bmatrix} -\frac{1}{L} \\ 0 \end{bmatrix} v_g \quad (4.14)$$

$$A_4 = \begin{bmatrix} 0 & -\frac{1}{L} \\ \frac{1}{C} & -\frac{1}{CR_L} \end{bmatrix} \begin{bmatrix} i_L \\ v_C \end{bmatrix}, \quad B_4 = \begin{bmatrix} -\frac{1}{L} \\ 0 \end{bmatrix} v_g \quad (4.15)$$

4.2 State-space averaging and linearization

State-space averaging and linearization help to analyze the system's time-variant components over time to average and linearize those varying elements for each state and determine the proposed system's continuous time function.

Using this waveform of the inductor voltage, and considering the full period T_s , the first operating state S_1 is determined by the value of ϕ . Similarly, S_2 would be $\frac{T_s}{2} - \phi$, S_3 would be $-\phi$, and lastly S_4 would be $-\frac{T_s}{2} - \phi$. For (ϕ) and $(\frac{T_s}{2} - \phi)$, these conversion is considered instead as an equivalent of these periods of time:

$$\phi(t) = \frac{d}{\frac{2}{T_s}} = \frac{dT_s}{2} \quad (4.16)$$

$$\frac{T_s}{2} - \phi(t) = \frac{T_s}{2} - \left(\frac{dT_s}{2}\right) = \frac{d'T_s}{2} \quad (4.17)$$

Table 4.1: Operating states time periods for DAB converter.

Operating State #	Time period
S_1 & S_3	$\frac{dT_s}{2}$
S_2 & S_4	$\frac{d'T_s}{2}$

The standard form of the state-space representation is:

$$\dot{x}(t) = Ax(t) + Bu(t) \quad (4.18)$$

$$y = Gx(t) + Hu(t) \quad (4.19)$$

All of each operating state matrices is multiplied by its time interval period:

$$\begin{aligned} \begin{bmatrix} \frac{d}{dt}i_L(t) \\ \frac{d}{dt}v_C(t) \end{bmatrix} &= \left(\frac{\frac{dT_s}{2}(A_1 + A_3)}{T_s} + \frac{\frac{d'T_s}{2}(A_2 + A_4)}{T_s} \right) \begin{bmatrix} i_L \\ v_C \end{bmatrix} + \\ &\left(\frac{\frac{dT_s}{2}(B_1 + B_2)}{T_s} + \frac{\frac{d'T_s}{2}(B_3 + B_4)}{T_s} \right) V_g \end{aligned} \quad (4.20)$$

$$\dot{x}(t) = \begin{bmatrix} 0 & \frac{2d-1}{L} \\ \frac{1}{C} & -\frac{1}{CR_L} \end{bmatrix} \begin{bmatrix} i_L \\ v_C \end{bmatrix} + \begin{bmatrix} \frac{1-2d}{L} \\ 0 \end{bmatrix} V_g \quad (4.21)$$

And, since we are only interested in the output voltage, and we do not have any feedthrough input in the circuit, therefore:

$$G = \begin{bmatrix} 0 & 1 \end{bmatrix}, \quad H = 0 \quad (4.22)$$

Perturbing and linearizing this result which means that all the time variant variables would equal to their DC component plus the AC small signal component, in the manner that:

$$i_L(t) = I_L + \hat{i}_L, \quad v_C(t) = V_C + \hat{v}_C, \quad v_g(t) = V_g + \hat{v}_g, \quad d = D + \hat{d}, \quad d' = D - \hat{d}$$

Perturb and linearization process is done thoroughly in APPENDIX B.

First order equations is only considered in this process so that DC and second order(non-linear) equations will be eliminated. Therefore as an (Equation B.5),

$$\begin{bmatrix} \hat{i}_L \\ \hat{v}_C \end{bmatrix} = \frac{(A_1 + A_3)}{2} \begin{bmatrix} I_L \hat{d} + \hat{i}_L D \\ V_C \hat{d} + \hat{v}_C D \end{bmatrix} + \frac{(A_2 + A_4)}{2} \begin{bmatrix} -I_L \hat{d} + \hat{i}_L D \\ -V_C \hat{d} + \hat{v}_C D \end{bmatrix} \\ + \left(\frac{B_1 + B_2}{2} \right) (V_g \hat{d} + \hat{v}_g D) + \left(\frac{B_3 + B_4}{2} \right) (-V_g \hat{d} + \hat{v}_g D) \quad (4.23)$$

$$\begin{aligned} \begin{bmatrix} \hat{i}_L \\ \hat{v}_C \end{bmatrix} &= \left(\frac{D}{2}\right) (A_1 + A_2 + A_3 + A_4) \begin{bmatrix} \hat{i}_L \\ \hat{v}_C \end{bmatrix} + \left(\frac{D}{2}\right) (B_1 + B_2 + B_3 + B_4) \hat{v}_g \\ &+ \left(\frac{1}{2} ((A_1 + A_3) - (A_2 + A_4)) \begin{bmatrix} I_L \\ V_C \end{bmatrix} + \frac{1}{2} ((B_1 + B_3) - (B_2 + B_4)) V_g \right) \hat{d} \end{aligned} \quad (4.24)$$

Which is equal to the form:

$$\hat{x} = A[\hat{x}] + B[\hat{v}_g] + E[\hat{d}] \quad (4.25)$$

Where:

$$E = ((A_1 + A_3) - (A_2 + A_4)) X_0 + ((B_1 + B_3) - (B_2 + B_4)) U_0 \quad (4.26)$$

$$E = \begin{bmatrix} \frac{2V_g}{L} \\ 0 \end{bmatrix} \quad (4.27)$$

4.3 Transfer function

Transfer functions are best to describe the relationship between the input and the output of a linear or time-variant system.

The AC small-signal solution of the system is:

$$\hat{x} = A \hat{x} + B \hat{v}_g + E \hat{d} \quad (4.28)$$

And since the equation is linearized, Laplace transformation can be applied resulting in:

$$\hat{X}(s) = (sI - A)^{-1} B \hat{U}(s) + (sI - A_0)^{-1} E \hat{d}(s) \quad (4.29)$$

Using this equation, line-to-output and control-to-output transfer functions could be derived as:

The line-to-output transfer function can be expressed as:

$$G_{vg}(s) = \frac{\hat{X}(s)}{\hat{U}(s)} \Big|_{\hat{d}(s)=0} = G (sI - A)^{-1} B \quad (4.30)$$

Which is found to be:

$$G_{vg}(s) = \frac{1 - 2D}{LC s^2 + \frac{L}{R} s + R(1 - 2D)} \quad (4.31)$$

And, the control-to-output transfer function can be expressed as:

$$G_{vd}(s) = \frac{\hat{X}(s)}{\hat{d}(s)} \Big|_{\hat{U}(s)=0} = G (sI - A)^{-1} E \quad (4.32)$$

Which is found to be:

$$G_{vd}(s) = \frac{2V_g}{LC s^2 + \frac{L}{R} s + R(1 - 2D)} \quad (4.33)$$

In this chapter, D is avoided to be 0.5, which it would make the system uncontrollable. This has been discussed in CHAPTER 3 and in (Figure 3.7).

CHAPTER 5: RESULTS

As mentioned previously, Simulink tool in MATLAB is used for this demonstration results to test the control logic and verify the output measurement.

First, the DAB converter topology, which has eight switching devices, a leakage inductor, a transformer, and input and output capacitors, was constructed.

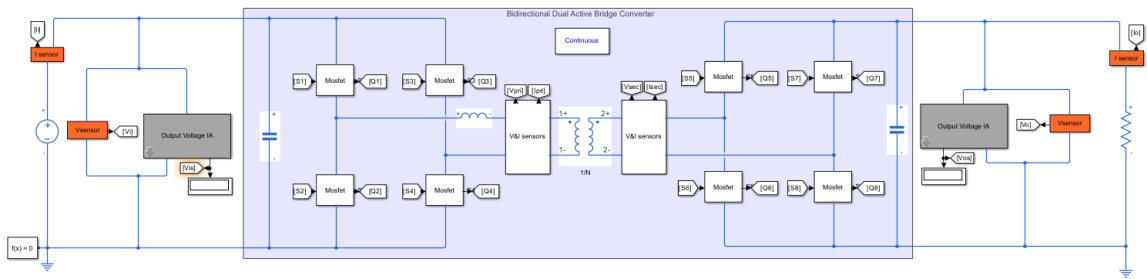


Figure 5.1: DAB Converter Simulation Circuit

Second, the control Unit block was connected to the converter, which contains the controllable gate drive signals, the control logic block diagram, and the SPS control method. It takes the voltage reference and the output voltage sensor's value as input and outputs the gate drive signals for the switching devices. Furthermore, a measurement scope was applied next to the control unit block to verify the phase-shifting waveform of the gate drive signal fed to the switching devices later.

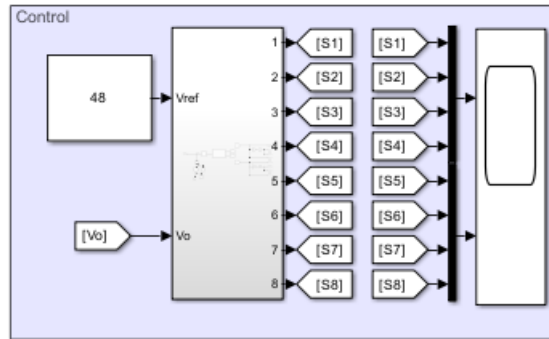


Figure 5.2: Simulation Control Unit

The control block diagram is constructed of the error between the voltage reference and the output voltage measurement, the PI controller, the transfer function of the DAB converter, and the SPS control logic block, which outputs to the first full bridge (FB1) and the second full bridge (FB2) of the converter.

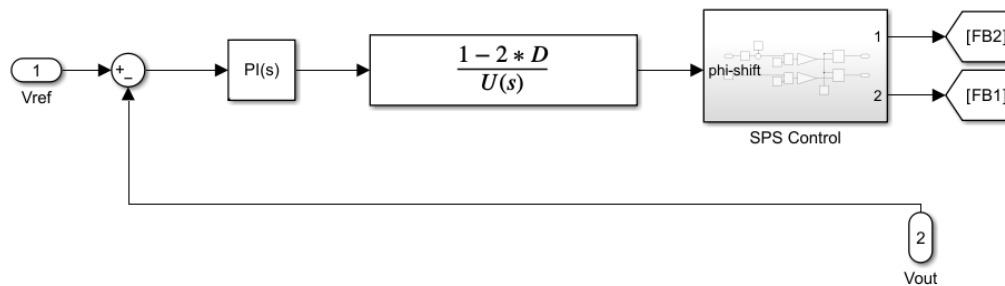


Figure 5.3: Simulation Control Block Diagram

Here is the SPS control logic, which translates the transfer function output into a phase-shift angle (ϕ) in terms of the frequency PWM output to shift the phase angle of one of the DAB converter bridges. The first leg of this block has an addition of 90 so that the control of (ϕ) is in the range of ($0 - 180^\circ$) instead of ($-90^\circ - 90^\circ$) to bypass Simulink limitations.

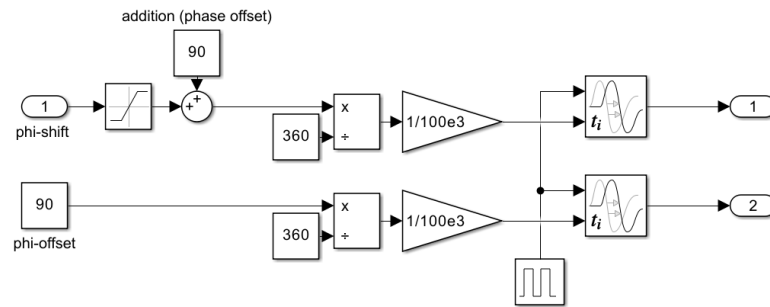


Figure 5.4: Phase Shifting Logic Subsystem of the Control Block Diagram

As the last section of the control unit block, the phase-shifting output is supplied FB1 and FB2 which feed to the switching devices in order to operate the DAB converter using this circuitry connection.

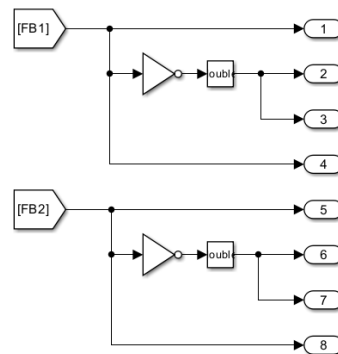


Figure 5.5: Simulation Switching Devices Signals

Lastly, a set of scope connections is put together for analysis and taking measurements.

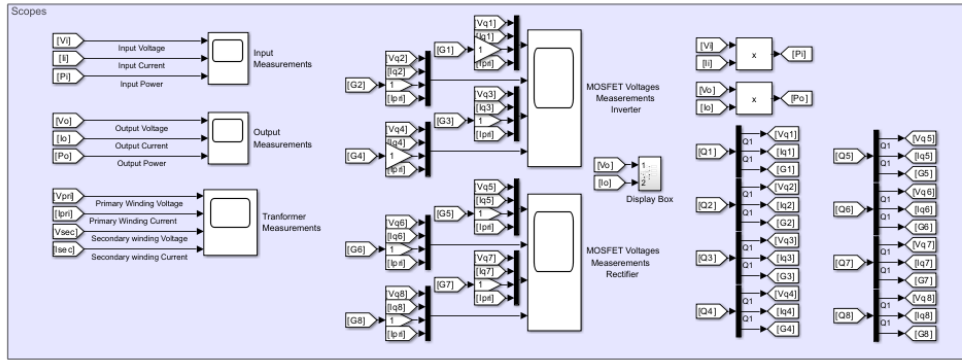


Figure 5.6: Simulation Scoping Probes

The DAB converter specifications used in this simulation are listed below in (Table 5.1):

Table 5.1: Converter Specifications for Simulink

Parameter	Variable	Value
Input Voltage	V_{in}	400 V
Output Voltage	V_o	48 V
Output Power	P_o	4000 W
Switching Frequency	f_{sw}	100 kHz
Transformer Ratio	n	8 : 1
Duty Ratio	D	0.4
Leakage Inductance	L	46.08 μH
Output Capacitor	C_o	177.78 μF
Load Resistance	R_L	0.576 Ω

5.1 Simulation Results

Output Measurements:

In this section, the output measurement simulation results are shown for different loading and input voltage varying conditions. Each figure is showing the output voltage, output current, and the output power accordingly as in red waveform. The blue color show the status of (ϕ), which is the controller variable, and how it behaves during transients and varying conditions.

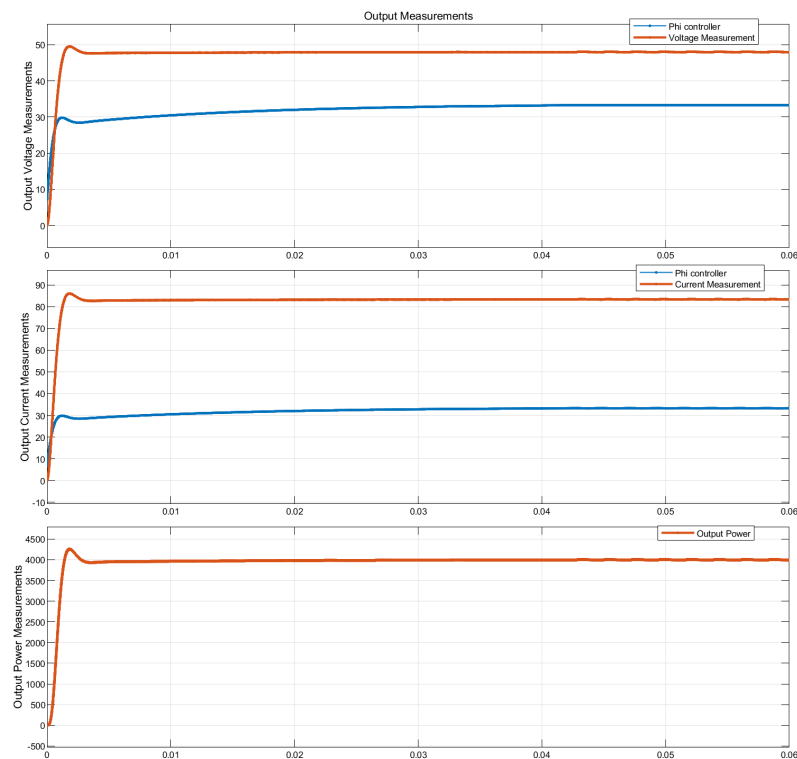


Figure 5.7: Simulation for Output Measurement at Nominal Load

Showing at Figure (5.7), in first scope, is the output voltage V_o measurement which is measured to be 48.05 V with a DC ripple of 0.16 V and reached steady-state in about 20 ms. In the second scope, is the output current I_o measurement which is measured to be 83.41 A with a DC ripple of 0.2 A and reached steady-state in about 20 ms.

And in the third scope, is the product of the first two measurements, which is the output power P_o measurement and it is measured to be 4,007 W and reached steady-state in about 2 ms.

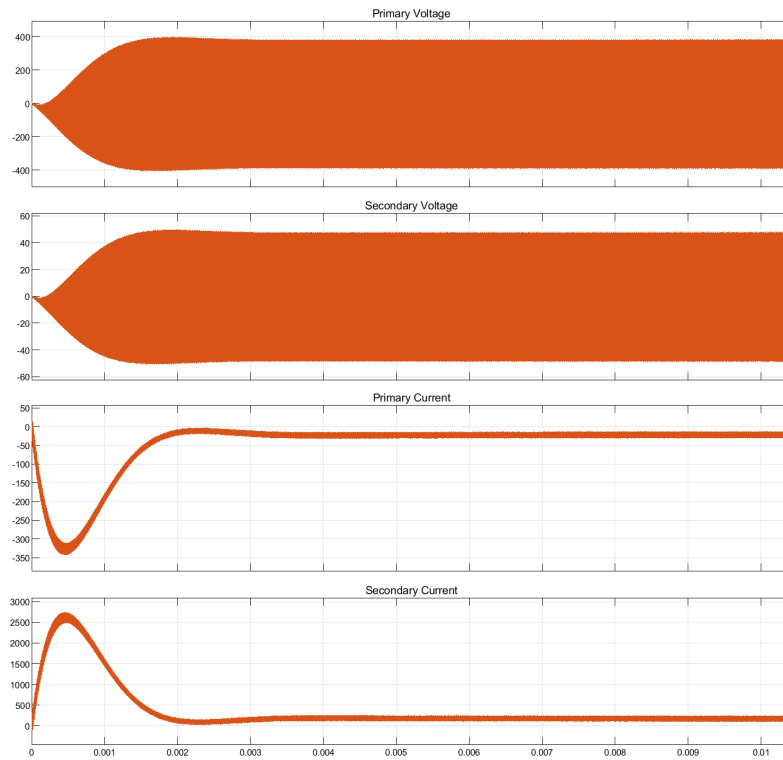


Figure 5.8: Simulation Transformer Measurements at Nominal Load

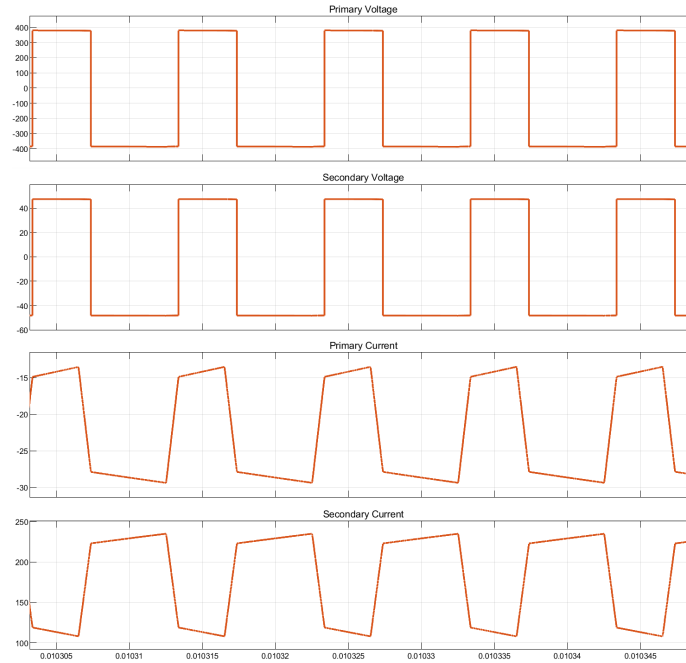


Figure 5.9: Simulation Transformer Waveform Characteristics

Figure (5.8) and (5.9), show the transformer measurements of the primary voltage V_p , secondary voltage V_s , primary current I_p , and the secondary current I_s at nominal load condition, where (Figure 5.8) shows the transformer output measurements, and (Figure 5.9) shows the waveform characteristics of the transformer measurements. The primary voltage is a square wave with phase shift effect of 396.1 V high, and -396.7 V low. The secondary voltage is a square wave with phase shift effect as well of 49.52 V high, and -49.58 V low.

The primary current is a trapezoidal waveform of high 21.1A , and -21.09 low. As the secondary current is a trapezoidal waveform of high 167.0A , and -168.8 low.

5.2 Varying Load and Input Voltage Conditions

In this section, the system stability was tested under different loading conditions and varying the input voltage.

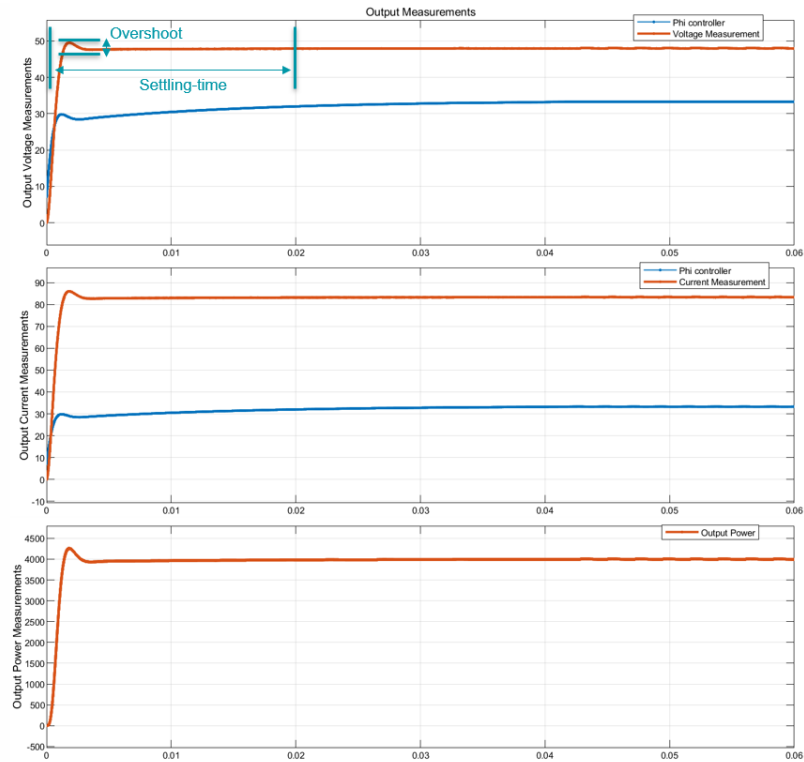


Figure 5.10: Output Measurements for Nominal Load Testing Condition.

At this waveform above, the system is running for a normal operation at nominal load condition where the system reach steady-state in 20ms and an overshoot value of 2.29% , where (ϕ) value is settling at 33° .

Then, the system will be disturbed at 0.02ms by varying the input voltage and testing different loads to analyze the control functionality by measuring the overshoot and settling time.

Here in (Figure 5.11), the system was tested at mid-point load, which has an overshoot of 2.92% and a settling time of 36 ms, where (ϕ) value is settling at 14°.

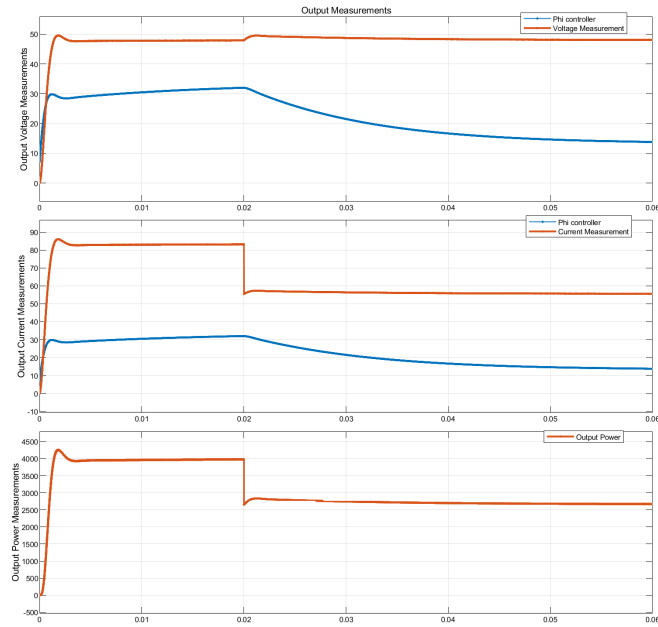


Figure 5.11: Output Measurements for Mid-point Load Testing Condition.

In (Figure 5.12), the system was tested at no-load condition, which has an overshoot of 11.76% and a settling time of 38.5 ms, where (ϕ) value is settling at -19° .

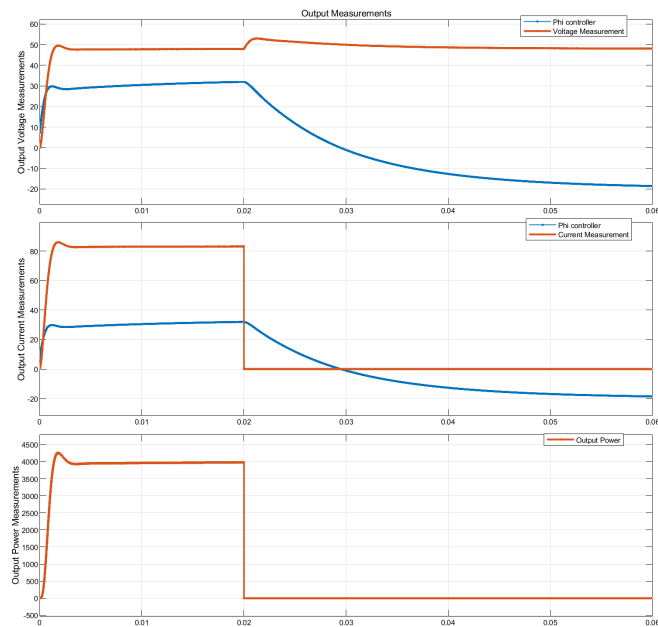


Figure 5.12: Output Measurements for No Load Testing Condition.

At this condition (Figure 5.13), the input voltage is stepped for +10%, which has an overshoot of 10.63% and a settling time of 29.7 *ms*, where (ϕ) value is settling at -15° .

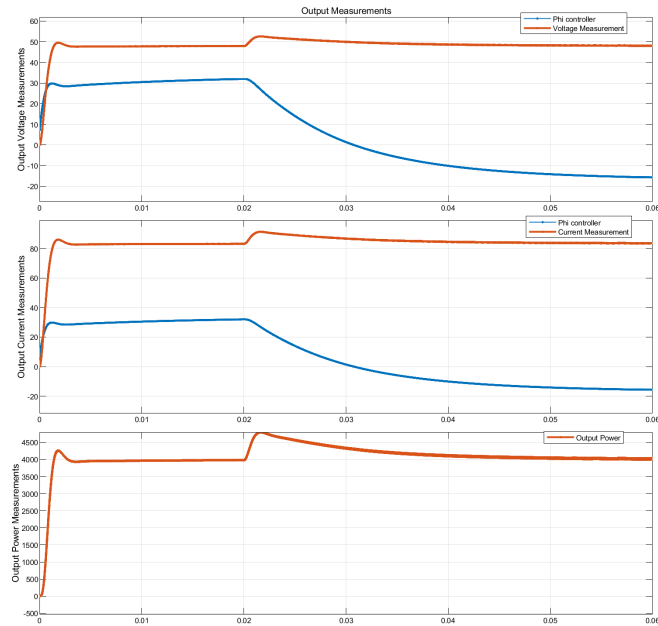


Figure 5.13: Output Measurements for 10% Input Voltage increment Testing Condition.

In addition, at this condition, the input voltage is stepped for +20%, which has an overshoot of 17.71% and a settling time of 39.6 *ms*, where (ϕ) value is settling at -81° .

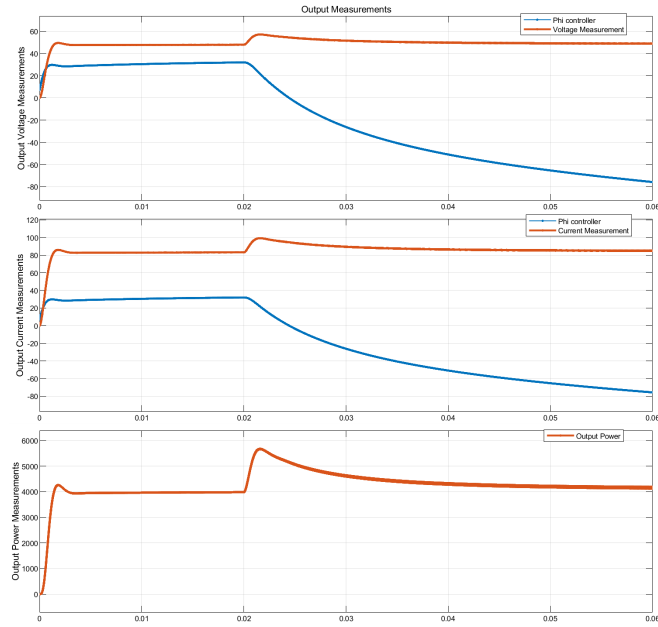


Figure 5.14: Output Measurements for 20% Input Voltage increment Testing Condition.

Table 5.2: Summary for different testing conditions

	Overshoot	Settling-time
Full Load	2.29%	20 <i>ms</i>
Mid-point Load	2.92%	36 <i>ms</i>
No Load	10.83%	38.5 <i>ms</i>
110% Input Voltage	10.63%	29.7 <i>ms</i>
120% Input Voltage	17.71%	39.6 <i>ms</i>

CHAPTER 6: CONCLUSIONS

In this master's thesis, a detailed analysis of DAB converter topology has been provided. A state-space representation and SPS control logic, design, averaging, and linearization were used for the control side.

One of the significant achievements of this thesis is validating the control logic proposed in Chapter 4, and by running the simulation for a varying load conditions or varying input voltage conditions which validates the control analysis results. The simulation results for different load and input voltage conditions were summarized in (Table 5.2).

While the presented data provide invaluable insights into the DAB converter, it is essential to mention that the experimental specifications were scaled down to accommodate the experiment's limitations. This research aims to achieve the full-scale objective of the converter specifications and conduct additional analysis in future work.

The future specification could be effectively used in many applications. For instance, the voltage-regulated level is commonly used in the EV field of expertise, which was an objective of this research.

In conclusion, this thesis comprehensively explores the DAB converter to understand its dynamics behavior, operation states, control strategies, and wide range of applications. The literature review chapter thoroughly lists significant contributions and developments of the DAB converter topology.

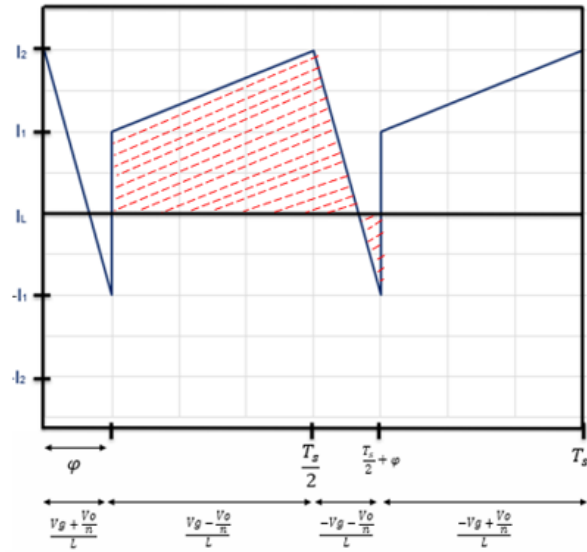
REFERENCES

- [1] R. De Doncker, D. Divan, and M. Kheraluwala, "A three-phase soft-switched high power density dc/dc converter for high power applications," in *Conference Record of the 1988 IEEE Industry Applications Society Annual Meeting*, pp. 796–805 vol.1, 1988.
- [2] M. L. Flach, C. A. d. Souza, L. G. Scherer, R. F. d. Camargo, and F. H. Dupont, "Application of the dab converter to a hybrid system for hydro-pv and battery," in *2018 13th IEEE International Conference on Industry Applications (INDUSCON)*, pp. 1327–1334, 2018.
- [3] R. T. Naayagi, A. J. Forsyth, and R. Shuttleworth, "Performance analysis of extended phase-shift control of dab dc-dc converter for aerospace energy storage system," in *2015 IEEE 11th International Conference on Power Electronics and Drive Systems*, pp. 514–517, 2015.
- [4] W. Shi, J. He, J. Song, and S. Yang, "Unified-phase-shift control method of dual active bridge dc-dc converter for data center application," in *2021 IEEE Sustainable Power and Energy Conference (iSPEC)*, pp. 3199–3203, 2021.
- [5] M. ElMenshawy and A. Massoud, "Multimodule dc-dc converters for high-voltage high-power renewable energy sources," in *2019 2nd International Conference on Smart Grid and Renewable Energy (SGRE)*, pp. 1–6, 2019.
- [6] N. Hou, Y. W. Li, and L. Ding, "Communicationless power management strategy for the multiple dab-based energy storage system in islanded dc microgrid," in *2020 IEEE Energy Conversion Congress and Exposition (ECCE)*, pp. 4656–4661, 2020.
- [7] H.-J. Choi, H.-P. Park, and J.-H. Jung, "Design methodology of dual active bridge converter for solid state transformer application in smart grid," in *2015 9th International Conference on Power Electronics and ECCE Asia (ICPE-ECCE Asia)*, pp. 196–201, 2015.
- [8] X. Li, W. Huang, B. Cui, and X. Jiang, "Inductance characteristics of the high-frequency transformer in dual active bridge converters," in *2019 22nd International Conference on Electrical Machines and Systems (ICEMS)*, pp. 1–5, 2019.
- [9] G. Xu, D. Sha, Y. Xu, and X. Liao, "Dual-transformer-based dab converter with wide zvs range for wide voltage conversion gain application," *IEEE Transactions on Industrial Electronics*, vol. 65, no. 4, pp. 3306–3316, 2018.
- [10] A. Amin, M. Shousha, A. ProdiÄ, and B. Lynch, "A transformerless dual active half-bridge dc-dc converter for point-of-load power supplies," in *2015 IEEE Energy Conversion Congress and Exposition (ECCE)*, pp. 133–140, 2015.

- [11] M. Kheraluwala, R. Gasgoigne, D. Divan, and E. Bauman, "Performance characterization of a high power dual active bridge dc/dc converter," in *Conference Record of the 1990 IEEE Industry Applications Society Annual Meeting*, pp. 1267–1273 vol.2, 1990.
- [12] H. Bai, C. C. Mi, and S. Gargies, "The short-time-scale transient processes in high-voltage and high-power isolated bidirectional dc/dc converters," *IEEE Transactions on Power Electronics*, vol. 23, no. 6, pp. 2648–2656, 2008.
- [13] B. Zhao, Q. Song, W. Liu, and Y. Sun, "Overview of dual-active-bridge isolated bidirectional dc/dc converter for high-frequency-link power-conversion system," *IEEE Transactions on Power Electronics*, vol. 29, no. 8, pp. 4091–4106, 2014.
- [14] C. Mi, H. Bai, C. Wang, and S. Gargies, "Operation, design and control of dual h-bridge-based isolated bidirectional dc-dc converter," *Power Electronics, IET*, vol. 1, no. 4, pp. 507 – 517, 2009.
- [15] B. Zhao, Q. Yu, and W. Sun, "Extended-phase-shift control of isolated bidirectional dc/dc converter for power distribution in microgrid," *IEEE Transactions on Power Electronics*, vol. 27, no. 11, pp. 4667–4680, 2012.
- [16] B. Zhao, Q. Song, and W. Liu, "Power characterization of isolated bidirectional dual-active-bridge dc/dc converter with dual-phase-shift control," *IEEE Transactions on Power Electronics*, vol. 27, no. 9, pp. 4172–4176, 2012.
- [17] F. Krismer and J. W. Kolar, "Accurate small-signal model for the digital control of an automotive bidirectional dual active bridge," *IEEE Transactions on Power Electronics*, vol. 24, no. 12, pp. 2756–2768, 2009.
- [18] F. Golnaraghi and B. Kuo, *Automatic Control Systems*. Wiley, 2009.
- [19] S. S. Shah and S. Bhattacharya, "A simple unified model for generic operation of dual active bridge converter," *IEEE Transactions on Industrial Electronics*, vol. 66, no. 5, pp. 3486–3495, 2019.
- [20] G. D. Demetriades and H.-P. Nee, "Characterization of the dual-active bridge topology for high-power applications employing a duty-cycle modulation," in *2008 IEEE Power Electronics Specialists Conference*, pp. 2791–2798, 2008.
- [21] M. Jimenez Carrizosa, J. Cortes, A. Benchaib, P. Alou, G. Damm, J. A. Cobos, and F. Lamnabhi-Lagarrigue, "Dc / dc converters as dc circuit-breakers in hvdc networks operation," in *2014 16th European Conference on Power Electronics and Applications*, pp. 1–10, 2014.

APPENDIX A: CAPACITOR SIZING CALCULATION

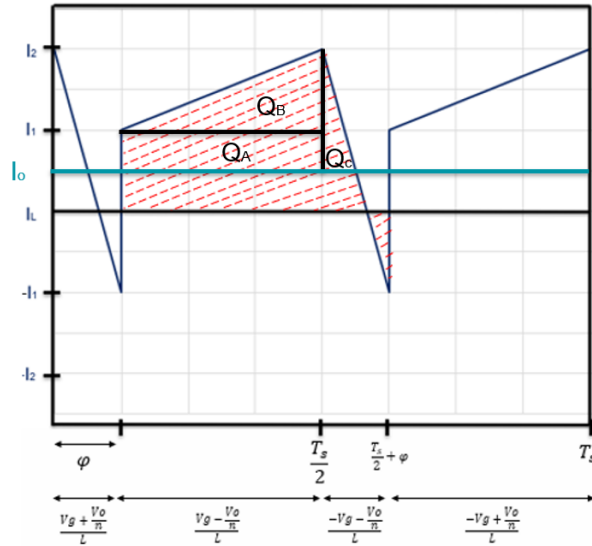
Using the output current waveform in (Figure 3.6):



And, using the capacitor formula in (Equation 3.10), which is:

$$I_o = \frac{\Delta Q}{n \frac{T_s}{2}} \quad (\text{A.1})$$

The output current is going to be a constant value at the average of the output current waveform. ΔQ needs to be calculated which is the difference between the output current and the capacitor current. A proper way to calculate this, is to divide this area into a square and a triangle as shown below.

Figure A.1: ΔQ Calculation

$$Q_A = \left(\frac{I_p}{n} - I_o\right) \left(\frac{T_s}{2} - \phi\right) \quad (\text{A.2})$$

$$Q_B = \frac{1}{2} \left(\frac{I_p}{n} - I_o\right) \left(\frac{T_s}{2} - \phi\right) \quad (\text{A.3})$$

$$Q_C = \frac{1}{2} \left(\frac{I_p}{n} - I_o\right) \left(\frac{\phi}{2}\right) \quad (\text{A.4})$$

$$Q_1 = Q_A + Q_B = \frac{3}{2} \left(\frac{I_p}{n} - I_o\right) \left(\frac{T_s}{2} - \phi\right) \quad (\text{A.5})$$

$$Q_2 = Q_C = \frac{1}{2} \left(\frac{I_p}{n} - I_o\right) \left(\frac{\phi}{2}\right) \quad (\text{A.6})$$

Using the following equivalent equations:

$$\frac{I_p}{n} = \frac{V_g D T_s}{2 f_{SW} L n} \quad (\text{A.7})$$

$$I_o = \frac{V_g D D' T_s}{2 f_{SW} L n} \quad (\text{A.8})$$

$$\phi = \frac{D T_s}{2} \quad (\text{A.9})$$

Q_1 and Q_2 could be calculated as follows:

$$Q_1 = \frac{3}{2} \left(\frac{V_g D T_s}{2 f_{SW} L n} - \frac{V_g D D' T_s}{2 f_{SW} L n} \right) \left(\frac{T_s}{2} - \frac{D T_s}{2} \right) \quad (\text{A.10})$$

$$= \frac{3}{4} \frac{V_g D T_s^2}{2 f_{SW} L n} (1 - D') (1 - D) \quad (\text{A.11})$$

$$Q_1 = \frac{3}{4} \frac{V_g D^2 D' T_s^2}{2 f_{SW} L n} \quad (\text{A.12})$$

$$Q_2 = \frac{1}{4} \frac{V_g D^3 T_s^2}{2 f_{SW} L n} \quad (\text{A.13})$$

$$\Delta Q = Q_1 + Q_2 \quad (\text{A.14})$$

$$\Delta Q = \frac{3}{4} \frac{V_g D^2 D' T_s^2}{2 f_{SW} L n} + \frac{1}{4} \frac{V_g D^3 T_s^2}{2 f_{SW} L n} \quad (\text{A.15})$$

$$\Delta Q = \frac{V_g D^2 T_s^2}{2 f_{SW} L n} \quad (\text{A.16})$$

Finally, the output capacitance could be calculated using the formula:

$$C_o = \frac{\Delta Q}{2 \Delta V_o} \quad (\text{A.17})$$

APPENDIX B: STATE-SPACE PERTURBING AND LINEARIZATION

Simplifying the previous equation (Equation 4.20):

$$\begin{aligned} \begin{bmatrix} \frac{d}{dt} i_L(t) \\ \frac{d}{dt} v_C(t) \end{bmatrix} &= \left(\frac{\frac{DT_s}{2}(A_1 + A_3)}{T_s} + \frac{\frac{D'T_s}{2}(A_2 + A_4)}{T_s} \right) \begin{bmatrix} i_L \\ v_C \end{bmatrix} \\ &+ \left(\frac{\frac{DT_s}{2}(B_1 + B_2)}{T_s} + \frac{\frac{D'T_s}{2}(B_3 + B_4)}{T_s} \right) V_g \end{aligned} \quad (\text{B.1})$$

$$\begin{aligned} \begin{bmatrix} \frac{d}{dt} i_L(t) \\ \frac{d}{dt} v_C(t) \end{bmatrix} &= \left(\frac{D(A_1 + A_3)}{2} + \frac{D'(A_2 + A_4)}{2} \right) \begin{bmatrix} i_L \\ v_C \end{bmatrix} \\ &+ \left(\frac{D(B_1 + B_2)}{T_s} + \frac{D'(B_3 + B_4)}{2} \right) V_g \end{aligned} \quad (\text{B.2})$$

$$\begin{aligned} \begin{bmatrix} \frac{d}{dt} i_L(t) \\ \frac{d}{dt} v_C(t) \end{bmatrix} &= \frac{(A_1 + A_3)}{2} \begin{bmatrix} i_L D \\ v_C D \end{bmatrix} + \frac{(A_2 + A_4)}{2} \begin{bmatrix} i_L D' \\ v_C D' \end{bmatrix} \\ &+ \left(\frac{B_1 + B_2}{2} \right) V_g D + \left(\frac{B_3 + B_4}{2} \right) V_g D' \end{aligned} \quad (\text{B.3})$$

Perturbing and linearizing:

$$\begin{aligned} \begin{bmatrix} \frac{d}{dt} (I_L + \hat{i}_L) \\ \frac{d}{dt} (V_C + \hat{v}_C) \end{bmatrix} &= \frac{(A_1 + A_3)}{2} \begin{bmatrix} (I_L + \hat{i}_L) (D + \hat{d}) \\ (V_C + \hat{v}_C) (D + \hat{d}) \end{bmatrix} + \frac{(A_2 + A_4)}{2} \begin{bmatrix} (I_L + \hat{i}_L) (D - \hat{d}) \\ (V_C + \hat{v}_C) (D - \hat{d}) \end{bmatrix} \\ &+ \left(\frac{B_1 + B_2}{2} \right) (V_g + \hat{v}_g) (D + \hat{d}) + \left(\frac{B_3 + B_4}{2} \right) (V_g + \hat{v}_g) (D - \hat{d}) \end{aligned} \quad (\text{B.4})$$

This would result into the below equation which have DC and AC small signal components.

$$\begin{aligned}
\begin{bmatrix} \frac{d}{dt}(\cancel{I_L} + \hat{i}_L) \\ \frac{d}{dt}(\cancel{V_C} + \hat{v}_C) \end{bmatrix} &= \frac{(A_1 + A_3)}{2} \begin{bmatrix} \cancel{I_L} \cancel{D} + I_L \hat{d} + \hat{i}_L D + \cancel{\hat{i}_L} \cancel{d} \\ \cancel{V_C} \cancel{D} + V_C \hat{d} + \hat{v}_C D + \cancel{\hat{v}_C} \cancel{d} \end{bmatrix} + \\
&\frac{(A_2 + A_4)}{2} \begin{bmatrix} \cancel{I_L} \cancel{D} - I_L \hat{d} + \hat{i}_L D - \cancel{\hat{i}_L} \cancel{d} \\ \cancel{V_C} \cancel{D} - V_C \hat{d} + \hat{v}_C D - \cancel{\hat{v}_C} \cancel{d} \end{bmatrix} \\
+ \left(\frac{B_1 + B_2}{2} \right) (\cancel{V_g} \cancel{D} + V_g \hat{d} + \hat{v}_g D + \cancel{\hat{v}_g} \cancel{d}) &+ \left(\frac{B_3 + B_4}{2} \right) (\cancel{V_g} \cancel{D} - V_g \hat{d} + \hat{v}_g D - \cancel{\hat{v}_g} \cancel{d}) \quad (\text{B.5})
\end{aligned}$$

First order equations is only considered in this process so that DC and second order(non-linear) equations will be eliminated. Therefore,

$$\begin{aligned}
\begin{bmatrix} \hat{i}_L \\ \hat{v}_C \end{bmatrix} &= \frac{(A_1 + A_3)}{2} \begin{bmatrix} I_L \hat{d} + \hat{i}_L D \\ V_C \hat{d} + \hat{v}_C D \end{bmatrix} + \frac{(A_2 + A_4)}{2} \begin{bmatrix} I_L \hat{d} + \hat{i}_L D \\ V_C \hat{d} + \hat{v}_C D \end{bmatrix} \\
&+ \left(\frac{B_1 + B_2}{2} \right) V_g \hat{d} + \hat{v}_g D + \left(\frac{B_3 + B_4}{2} \right) - V_g \hat{d} + \hat{v}_g D \quad (\text{B.6})
\end{aligned}$$